


## Article

# Adhesion and Electron Properties of Quasi-2D Mo<sub>2</sub>C, Ti<sub>2</sub>C, and V<sub>2</sub>C MXene Flakes after Van Der Waals Adsorption of Alcohol Molecules: Influence of Humidity

Dmitry A. Kolosov<sup>1</sup>, Semyon G. Levitsky<sup>1</sup> and Olga E. Glukhova<sup>1,2,\*</sup> 

<sup>1</sup> Department of Physics, Saratov State University, Astrakhanskaya Street 83, 410012 Saratov, Russia; kolosovda@bk.ru (D.A.K.); levickysg@gmail.com (S.G.L.)

<sup>2</sup> Laboratory of Biomedical Nanotechnology, I.M. Sechenov First Moscow State Medical University, Trubetskaya Street 8-2, 119991 Moscow, Russia

\* Correspondence: glukhovae@info.sgu.ru; Tel.: +7-84-5251-4562

**Abstract:** The adhesive properties of new materials quasi-2D Mo<sub>2</sub>C, Ti<sub>2</sub>C, and V<sub>2</sub>C MXene flakes play a crucial role (1) in the formation of highly efficient lubricants; (2) in the development of highly sensitive gas sensors. This paper reports DFT modeling of adsorption of alcohol molecules onto the surface of quasi-2D nanometer-thick flakes of MXenes. The parameters characterizing the adsorption mechanism were the analyte+surface binding energy, Fermi energy, and electrical conductivity. Due to the presence of water in the environment, MXene surfaces with varying degrees of humidity were studied, and the patterns of analyte adsorption onto a wet surface were investigated. A different approach to adhesion of alcohols for wet and dry surfaces has been established in this study.

**Keywords:** MXenes; Mo<sub>2</sub>C; Ti<sub>2</sub>C; V<sub>2</sub>C; sensors; DFT; humidity



**Citation:** Kolosov, D.A.; Levitsky, S.G.; Glukhova, O.E. Adhesion and Electron Properties of Quasi-2D Mo<sub>2</sub>C, Ti<sub>2</sub>C, and V<sub>2</sub>C MXene Flakes after Van Der Waals Adsorption of Alcohol Molecules: Influence of Humidity. *Lubricants* **2022**, *10*, 159. <https://doi.org/10.3390/lubricants10070159>

Received: 31 May 2022

Accepted: 15 July 2022

Published: 17 July 2022

**Publisher's Note:** MDPI stays neutral with regard to jurisdictional claims in published maps and institutional affiliations.



**Copyright:** © 2022 by the authors. Licensee MDPI, Basel, Switzerland. This article is an open access article distributed under the terms and conditions of the Creative Commons Attribution (CC BY) license (<https://creativecommons.org/licenses/by/4.0/>).

## 1. Introduction

Currently, MXenes that represent nitrides and carbides of transition metals are very popular in their niche among promising 2D materials due to their unique properties and broad field of application [1–4]. Grützmacher et al. showed that titanium carbide-based MXene deposited on stainless steel substrates could be a solid lubricant, exhibiting a six-fold reduction in friction and an ultra-low wear rate over 100,000 sliding cycles [5].

Marian et al. [6] evaluated the effect of Ti<sub>3</sub>C<sub>2</sub>Tx nanosheets on energy efficiency and operating time when used as a solid lubricant in highly loaded rolling and sliding machine elements. In this work, a decrease in the friction torque by up to 3.2 times, an increase in the service life by a factor of 2.1, and a decrease in the linear cumulative wear rate by up to 2.9 were observed compared to studies without coating with Ti<sub>3</sub>C<sub>2</sub>Tx nanosheets. Researchers have also examined the role of moisture when using MXenes as solid lubricants. The paper [7] shows the outstanding anti-wear properties of Ti<sub>3</sub>C<sub>2</sub>Tx nanosheets operating under conditions of moderate contact pressure and low humidity. The authors state that end groups and the amount of intercalated water are the determining parameters for interfacial strength and friction and wear characteristics. Another paper [8] highlights the influence of humidity in tribological experiments. Compared to the polished steel reference, the Ti<sub>3</sub>C<sub>2</sub>Tx nanoparticles caused a significant friction reduction of about 300% at a very low humidity level of 4%. The authors also state that Ti<sub>3</sub>C<sub>2</sub>Tx nanoparticles have demonstrated their effectiveness against various wear modes, including adhesive, abrasive, and tribochemical wear. Mochalin et al. [9] investigated the stability of MXene Ti<sub>3</sub>C<sub>2</sub>Tx and Ti<sub>2</sub>CTx in water and anhydrous colloidal solutions, and they showed that water, rather than O<sub>2</sub>, plays a key role in the reactions leading to the decomposition of MXene, and it is from water, not oxygen, that MXene must be protected. Li et al. fabricated piezoresistive pressure sensors based on hydrophobic organic/inorganic hybrid

films composed of the natural elastic poly (vinylidene fluoride) trifluoroethylene and multilayer  $Ti_3C_2Tx$  [10]. Due to viscoelasticity and hydrophobic properties, the obtained films demonstrated a very high gauge factor of  $817.4 \text{ kPa}^{-1}$  in a range from 0.072 to 0.74 kPa,  $2213.68 \text{ kPa}^{-1}$  from 0.74 to 3.083 kPa, and a rapid response time of 16 ms, as well as long-term stability. At the same time, the problem of developing chemoresistive sensors remains very relevant. In almost all areas of human activity, it is necessary to control the air for the presence of harmful substances and gases, control humidity in residential premises, and control the composition of the air during mining and, of course, in order to ensure fire safety. In this respect, the two-dimensional layered morphology, tunable surface through functionalization, low-noise metallic conductivity, and mechanical flexibility make MXenes promising materials for chemoresistive sensors. The most suitable for sensor application is  $Ti_3C_2Tx$ , which has high sensitivity to alcohols, ketones, and ammonia at concentrations of less than 100 ppb [11–14]. Besides  $Ti_3C_2Tx$ ,  $Mo_2CTx$  and  $V_2CTx$  MXenes are also in demand.  $Mo_2CTx$  can be successfully synthesized by selective removal of Ga from  $Mo_2Ga_2C$  [15]. Guo et al. studied  $Mo_2CTx$  properties from the point of determination of gas mixtures of hydrocarbons and volatile organic compounds [16]. In one study [17], high-purity  $V_2CTx$  MXenes were successfully synthesized using only NaF + HCl etchant solution. The authors claim that NaF + HCl has better exfoliating power than NaF + HF and KF + HCl. Furthermore, a suitable condition is etching in a solution of NaF + HCl at  $90^\circ\text{C}$  for 72 h.  $V_2CTx$  MXenes also have a high rate of mixture detection [18–20]. An ultra-sensitive gas sensor was designed based on  $V_2CTx$  with a response for polar and non-polar gases with concentrations of about 100 ppm [21].

As mentioned above, there is a lot of research on the impact of moisture on lubricants. As can be seen, the development of gas sensors based on MXenes is an important branch of modern science. However, at present, little attention has been paid to assessing the effect of humidity on the chemoresistive response of various MXene compounds. In our work, we performed a theoretical study of chemoresistive properties of MXenes based on titanium, vanadium and molybdenum carbides in the presence of analyte (ethanol).

## 2. Materials and Methods

The ab initio study of MXenes was performed using density functional theory (DFT) implemented in the Siesta 4.1.5 code [22,23]. To describe the exchange-correlation effects taking into account the van der Waals interaction, the vdW-DF approximation with the exchange–correlation functional of Berland and Hildgaard (BH) was used [24]. This functional showed good accuracy for a wide range of materials [25]. For the ground state optimization of MXenes, we applied a basis set of valence-split DZP (Double Zeta Plus Polarization) orbitals including polarization functions. A 3D periodic box was used (in the Siesta software package, all calculations can be performed only in a 3D periodic box). The Brillouin zone was sampled by Monkhorst-Pack scheme  $5 \times 5 \times 1$  [26]. In the X and Y directions, the lattice vectors were: 15.377 Å for  $Ti_2C$ ; 14.741 Å for  $V_2C$ ; and 14.425 Å for  $Mo_2C$ . The size of the box in the third direction Z was taken as equal to 100 Å to exclude any interaction between the layers in this direction. Geometrical optimization of atom coordinates and lattice vectors was performed, and the minimization of the total energy was carried out using the Hellman–Feynman forces, taking into account the Bullet-type corrections and using the modified Broyden’s algorithm [27], with the condition that the forces acting on the atoms of the structure were no more than  $0.04 \text{ eV}/\text{Å}$ , where the resulting lattice vectors were: 15.377 Å for  $Ti_2C$ ; 14.741 Å for  $V_2C$ ; and 14.425 Å for  $Mo_2C$ .

The vacuum layer over the MXenes’ surface was about 100 Å. The cutoff of the real space grid was 350 Ry.

The binding energy was calculated using Formula (1):

$$E_{\text{Binding energy}} = E_{\text{MXene}+\text{H}_2\text{O}+\text{Ethanol}} - (E_{\text{MXene}} + E_{\text{H}_2\text{O}} + E_{\text{Ethanol}}) \quad (1)$$

To calculate the chemical resistive response, the Transiesta package was applied. The calculation of conductivity was performed within the framework of the Landauer–Buttiker formalism [28] in accordance with the formula below:

$$G = \frac{2e}{h} \int_{-\infty}^{\infty} T(E) F_T(E - E_F) dE \quad (2)$$

where  $E_F$ —Fermi energy of contact material;  $e$ —electron's charge;  $h$ —Planck's constant;  $F_T$ —function that determines the value of the temperature broadening;  $T(E)$ —transmission function that can be calculated as follows:

$$T(E) = \text{Tr} \left[ \Gamma_L(E) G(E) \Gamma_R(E) G^\dagger(E) \right] \quad (3)$$

where  $G^\dagger(E)$ ,  $G(E)$  are the advanced and retarded Green matrices that describe the contact of object with the electrodes, respectively, and  $\Gamma_L(E)$ ,  $\Gamma_R(E)$  are the level broadening matrices for the source and drain, respectively. The level broadening matrices are calculated as follows:

$$\Gamma_{L/R}(E) = i \left( \Sigma_{L/R}(E) - \Sigma_{L/R}^\dagger(E) \right) \quad (4)$$

where  $\Sigma_{L/R}$  eigenenergy matrices of the left and right electrodes. Green's matrices are calculated as

$$G(E) = \frac{1}{(ES_C - H_C - \Sigma_L(E) - \Sigma_R(E))} \quad (5)$$

where  $S_C$  is the atomic orbital overlap matrix of the conducting channel;  $E$ —Energy of conductive channel;  $H_C$ —Hamiltonian of conductive channel.

The transport properties were calculated in several stages: (1) obtaining the surface Green–Keldysh functions of the semi-infinite left and right electrodes; (2) calculating the Hamiltonian of the scattering region. The electrodes belonged to the same atomic supercells as the structure of the scattering region.

### 3. Results and Discussion

#### 3.1. Atomistic Models of MXene 2D-Films

In this study, three atomistic models of MXenes were considered: (1)  $\text{Ti}_2\text{C}$ ; (2)  $\text{V}_2\text{C}$ ; (3)  $\text{Mo}_2\text{C}$  (Figure 1). Structures of  $\text{Ti}_2\text{C}$  and  $\text{V}_2\text{C}$  represented 1T phase of MXenes,  $\text{Mo}_2\text{C}$ —2H phase. Initially, we considered the atomic configurations of the minimum possible supercells with lattice vectors: 3.07 Å for  $\text{Ti}_2\text{C}$ ; 2.95 Å for  $\text{V}_2\text{C}$ ; and 2.89 Å for  $\text{Mo}_2\text{C}$ . Then, after geometric relaxation of atomic coordinates and lattice vectors, the structures were expanded by enlarging the number of supercells. In the result, atomistic supercells with the following lattice vectors were obtained: 15.377 Å for  $\text{Ti}_2\text{C}$ ; 14.741 Å for  $\text{V}_2\text{C}$ ; and 14.425 Å for  $\text{Mo}_2\text{C}$ . The increase in the area of the considered objects was caused by the required landing of water and ethanol molecules on the MXenes' surface. The paper considers the case of landing on the surface of MXenes of one and seven water molecules. To assess the effect of water molecules during gas adsorption, an ethanol molecule was located both on a clean, anhydrous MXene surface and in the presence of water molecules. Further, in order to evaluate the chemoresistive response, the transmission function calculations were performed for each considered case including the calculation of the electrical conductivity of pure MXene films. The electrodes and the scattering region were represented by the same atomistic models corresponding to Figure 2. Later, the electrical conductivity of each atomistic model was calculated by Equation (1).

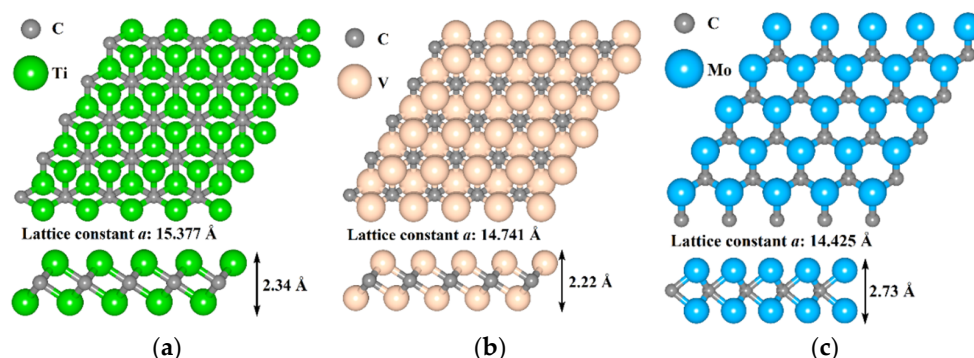


**Figure 1.** Atomistic models of pure MXene films: (a)  $\text{Ti}_2\text{C}$ ; (b)  $\text{V}_2\text{C}$ ; (c)  $\text{Mo}_2\text{C}$ .

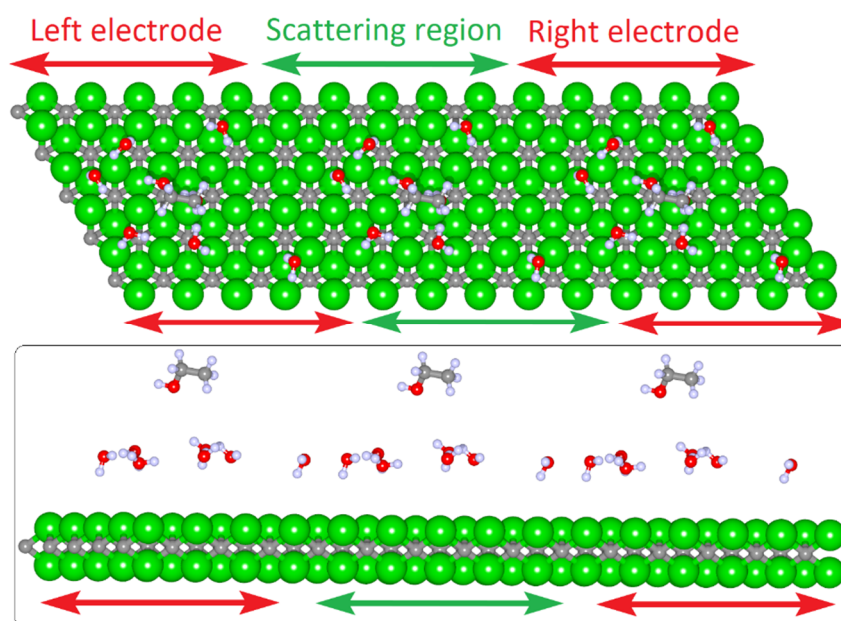


**Figure 2.** The calculation of electrical conductivity for atomistic models of titanium carbide in the presence of seven water molecules and an ethanol molecule. The electrodes are indicated on the left and right, the scattering region is in the center.

### 3.2. Electronic Properties

This section examines the density of state (DOS) of MXene supercells (Figure 3). The considered MXenes demonstrated a metallic type of conductivity with no band gap at the Fermi level, which agrees with previous studies [29–31].  $\text{Ti}_2\text{C}$  MXene had the biggest peak at the Fermi level with a value of  $100 \text{ eV}^{-1}$ . A high value of DOS at the Fermi level indicated good electric and conductive properties of this material, which will be further confirmed by transmission function calculation. As seen from Figure 3a–c, landing of analyte shifted the Fermi level. The landing of one water molecule practically did not change the DOS of pure  $\text{Ti}_2\text{C}$  MXene film.  $\text{V}_2\text{C}$  and  $\text{Mo}_2\text{C}$  MXenes were more sensitive to the presence of the water molecule and the Fermi level shifted more. At the same time, DOS plots of  $\text{V}_2\text{C}$  and  $\text{Mo}_2\text{C}$  MXenes with seven water molecules were close to pure films. It should be noted that attachment of ethanol did not change the DOS plot of supercells with seven molecules. Table 1 shows the Fermi level for all considered cases. The Fermi energy of  $\text{Ti}_2\text{C}$  MXene in the presence of ethanol shifted to the valence band region by 89 meV, while the Fermi energy of  $\text{V}_2\text{C}$  and  $\text{Mo}_2\text{C}$  MXenes shifted to the conduction band region by 54 meV and 115 meV, respectively.  $\text{Mo}_2\text{C}$  was more receptive to the ethanol molecule in terms of resistance change, as compared to the  $\text{Ti}_2\text{C}$  and  $\text{V}_2\text{C}$  MXenes, as shown in Figure 3d. For the case of one water molecule and one ethanol molecule, the Fermi energy

of  $Ti_2C$  shifted by 63 meV, while  $V_2C$  showed an almost unchanged value for the Fermi energy ( $\sim 6$  meV).  $Mo_2C$ , on the contrary, showed the largest shift in Fermi energy, equal to 184 meV. As shown below, the shift of Fermi energy towards the conduction band does not lead to an increase in electrical conductivity, since in this case, the number of electronic states decreases.

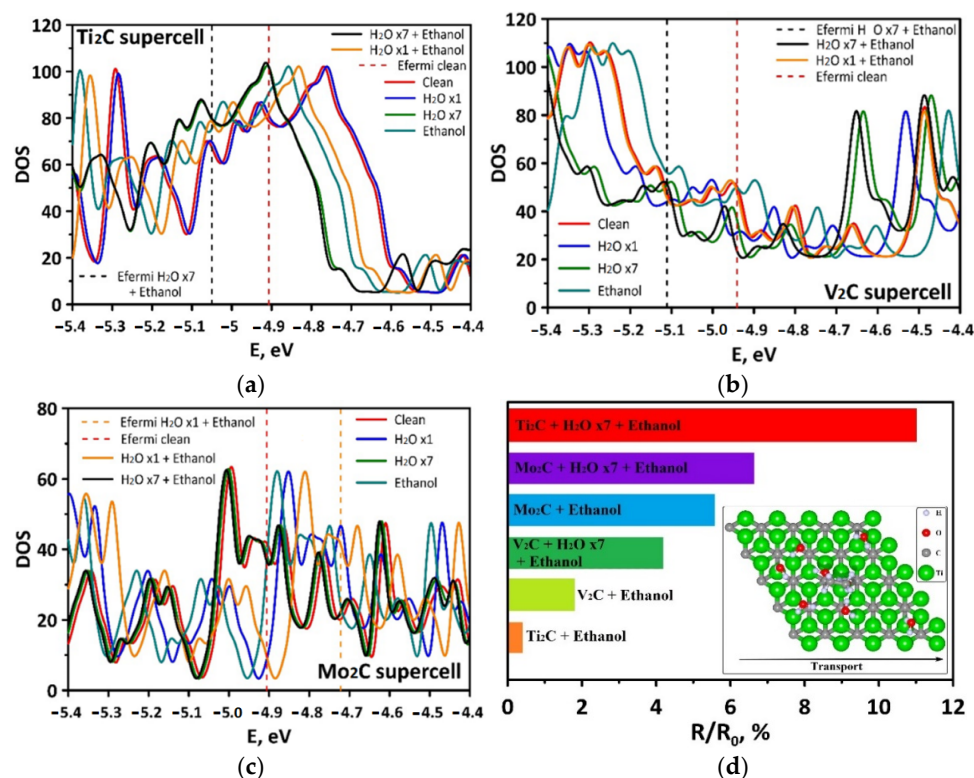


**Figure 3.** DOS plots of considered MXene molecules (a–c) and scale of resistance change after ethanol attachment (d).

**Table 1.** Fermi level of MXene films after interaction with ethanol and water.

Structure	$E_F$ , eV ( $Ti_2C$ )	$E_F$ , eV ( $V_2C$ )	$E_F$ , eV ( $Mo_2C$ )
Pure MXene film	−4.907	−4.941	−4.906
MXene + 1 water molecule	−4.899	−4.992	−4.764
MXene + 7 water molecules	−5.048	−5.094	−4.913
MXene + ethanol molecule	−4.996	−4.887	−4.791
MXene + 1 water molecule + ethanol molecule	−4.970	−4.947	−4.722
MXene + 7 water molecules + ethanol molecule	−5.050	−5.111	−4.918

To identify the patterns of Fermi level change after analyte landing, the distribution of charge density along supercell atoms was calculated by Mulliken procedure [32] (Figure 4). As the figure shows, the distribution of charge densities for one and seven water molecules differed. With the presence of one water molecule and one ethanol molecule, the surface of  $Ti_2C$  and  $Mo_2C$  MXenes demonstrated higher redistribution in place of water landing, while the charge distribution on the  $V_2C$  surface remained almost the same. This explains the small change in the Fermi energy of MXene  $V_2C$  during the simultaneous landing of one water molecule and one ethanol molecule. With the presence of seven water molecules,  $Ti_2C$  and  $Mo_2C$  MXenes still had a bigger charge redistribution on its surface than  $V_2C$  (Figure 4d–f) where vanadium atoms had an almost similar charge. In this case,  $Ti_2C$  donated 0.083e to the water molecules,  $Mo_2C$  was 0.079e, and  $V_2C$  donated 0.009 electrons, which is an order of magnitude less than  $Mo_2C$  and  $Ti_2C$ . Figure 5 shows the difference in charge density of the MXenes under consideration. As can be seen from the figure, for all

cases, an overlap of electron density is observed. Table 2 shows the charge transfer value for all considered cases. Here, the negative value of the excess charge indicates that the analyte or water molecule donates part of the charge to the MXene film. This charge is distributed over the entire surface of the MXene. With a positive value of the excess charge, the reverse process occurs: water molecules take on part of the charge from the MXene film. As seen from Table 2,  $V_2C$  has the lowest excess charge in the presence of the water molecules, but for the pure surface, its charge transfer is maximal.

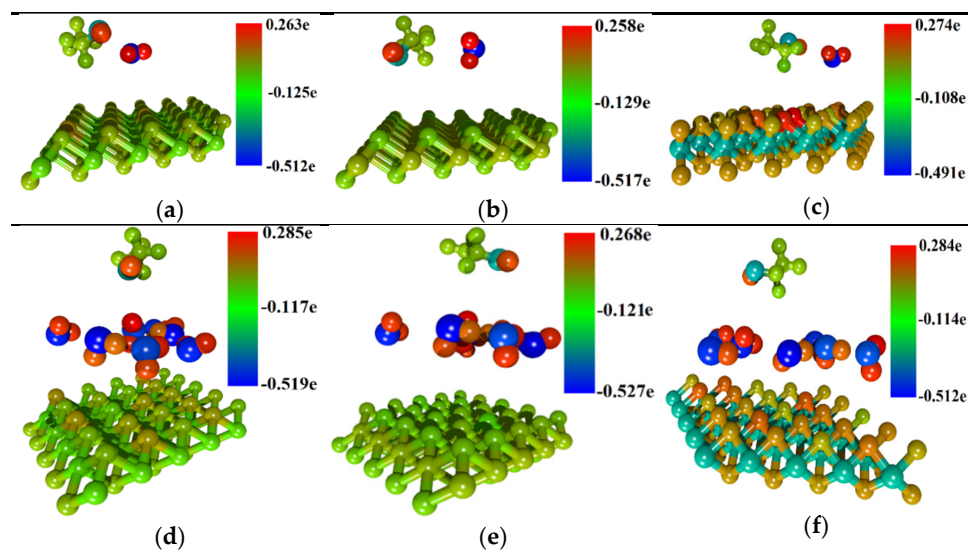


**Figure 4.** Charge distribution along the supercells atoms according to Mulliken procedure: (a)  $Ti_2C + H_2O \times 1 + Ethanol$ ; (b)  $V_2C + H_2O \times 1 + Ethanol$ ; (c)  $Mo_2C + H_2O \times 1 + Ethanol$ ; (d)  $Ti_2C + H_2O \times 7 + Ethanol$ ; (e)  $V_2C + H_2O \times 7 + Ethanol$ ; (f)  $Mo_2C + H_2O \times 7 + Ethanol$ .

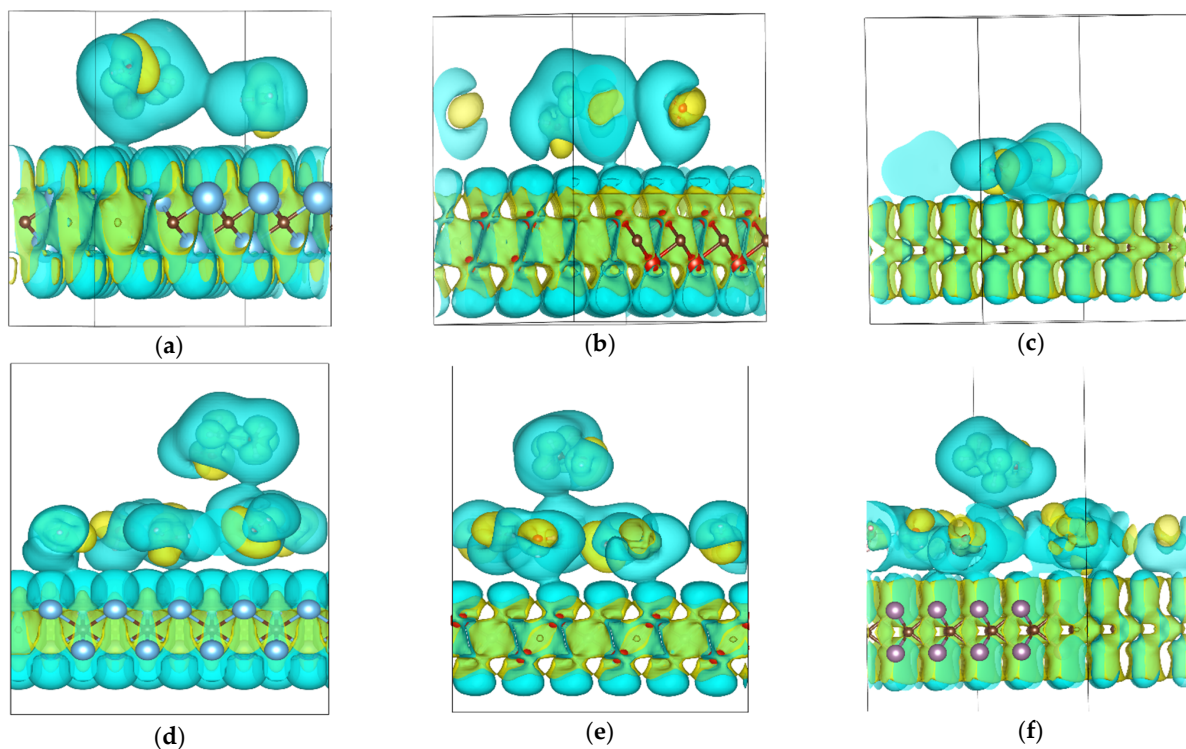


**Figure 5.** Charge Density Difference MXene: (a)  $Ti_2C + H_2O \times 1 + Ethanol$ ; (b)  $V_2C + H_2O \times 1 + Ethanol$ ; (c)  $Mo_2C + H_2O \times 1 + Ethanol$ ; (d)  $Ti_2C + H_2O \times 7 + Ethanol$ ; (e)  $V_2C + H_2O \times 7 + Ethanol$ ; (f)  $Mo_2C + H_2O \times 7 + Ethanol$ .

**Table 2.** Charge transfer between MXene films and analyte.

Structure	Excess Charge, e- (Ti <sub>2</sub> C)	Excess Charge, e- (V <sub>2</sub> C)	Excess Charge, e- (Mo <sub>2</sub> C)
MXene + 1 water molecule	−0.010	−0.006	−0.021
MXene + 7 water molecules	0.014	0.011	0.054
MXene + ethanol molecule	−0.007	−0.015	−0.011
MXene + 1 water molecule + ethanol molecule	(−0.01) H <sub>2</sub> O (0.012) Ethanol	(−0.004) H <sub>2</sub> O (0.006) Ethanol	(−0.006) H <sub>2</sub> O (−0.014) Ethanol
MXene + 7 water molecules + ethanol molecule	(−0.008) H <sub>2</sub> O ×7 (0.006) Ethanol	(−0.009) H <sub>2</sub> O ×7 (0.0011) Ethanol	(−0.079) H <sub>2</sub> O ×7 (0.007) Ethanol

At the next change, a chemoresistive response was calculated for wet and dry surfaces of MXenes (Table 3). It can be seen that for seven water molecules on the surface of MXene, the chemoresistive response to the gas under study (ethanol) is almost completely blocked. In the presence of seven water molecules, the addition of ethanol changed resistance at 0.01% for Ti<sub>2</sub>C, 0.022% for V<sub>2</sub>C, and 0.048% for Mo<sub>2</sub>C. The presence of seven water molecules blocks a significant chemoresistant response. At the same time, the conductivity of films changed quite significantly in the wet medium in comparison to the pure one. For the Ti<sub>2</sub>C films, resistance increased at 11%, for V<sub>2</sub>C at 4.2%, and for Mo<sub>2</sub>C at 6.63%. Figure 3d demonstrates the scale of resistance change after ethanol attachment for wet and dry surfaces. The Ti<sub>2</sub>C film was the most significantly affected by a wet surface, while for the one ethanol molecule the chemoresistive response was only 0.45%. The chemoresistive response of the V<sub>2</sub>C at the ethanol molecule was 1.83%, and at the water surface, it was 4.22%. The Mo<sub>2</sub>C MXene showed the best chemoresistive response for the ethanol (5.64%) and the lower humidity influence than Ti<sub>2</sub>C. The results for Mo<sub>2</sub>C are in good agreement with earlier studies [33].

**Table 3.** Resistance of MXene films after interaction with water and ethanol.

Structure	R, Ohm (Ti <sub>2</sub> C)	R, Ohm (V <sub>2</sub> C)	R, Ohm (Mo <sub>2</sub> C)
MXene + 1 water molecule	886.1	2562.7	973.2
MXene + 7 water molecules	901.1	2604.8	1011.2
MXene + ethanol molecule	983.9	2670.3	1037.8
MXene + 1 water molecule + ethanol molecule	890.1	2609.5	1028.1
MXene + 7 water molecules + ethanol molecule	902.3	2613.3	1012.4

At the final stage the binding energy between MXenes and analyte was calculated (Table 4). The values of binding energies show that chemical bonds between MXenes and ethanol did not form and the main type of interaction is van der Waals. MXene Mo<sub>2</sub>C, when one molecule of water was planted, showed the highest binding energy equal to −0.132 eV. The same trend persists for seven water molecules (−1.287 eV), as well as seven water and ethanol molecules (−1.375 eV). The high binding energy explains the high chemoresistive response of Mo<sub>2</sub>C compared to Ti<sub>2</sub>C and V<sub>2</sub>C. At the same time, the binding energy of Ti<sub>2</sub>C equal to −0.129 eV does not provide advantages in chemisorption. Of all the MXenes considered in this paper, Ti<sub>2</sub>C showed the worst result in terms of chemoresistive response. V<sub>2</sub>C has the lowest binding energy for both one water molecule and seven water molecules, including the case of ethanol. When the surface is fully filled with the water (seven molecules), the binding energies were maximal. The low binding energies indicate the renewable operation of sensors when they are purged with inert gases for all the considered films. However, a wet surface can prevent the “cleaning” of the working surface.

**Table 4.** Binding energies of MXene films after interaction with water and ethanol.

Structure	Binding Energy, eV (Ti <sub>2</sub> C)	Binding Energy, eV (V <sub>2</sub> C)	Binding Energy, eV (Mo <sub>2</sub> C)
MXene + 1 water molecule	−0.068	−0.054	−0.132
MXene + 7 water molecules	−0.841	−0.601	−1.287
MXene + ethanol molecule	−0.129	−0.137	−0.051
MXene + 1 water molecule + ethanol molecule	−0.226	−0.136	−0.109
MXene + 7 water molecules + ethanol molecule	−1.132	−0.625	−1.375

#### 4. Conclusions

Thus, a predictive study of the humidity effect on the chemoresistive properties of MXene films on the base of titanium carbide, vanadium and molybdenum were performed by using the ab initio method. It was established that the chemoresistive response was caused by displacement of Fermi energy in relation to the initial position. In the case of a one water molecule on the surface of MXenes, it promoted a chemoresistant response comparable to that of an ethanol molecule. However, in the case of the landing of seven water molecules, the sensory properties of the films for the test gas were almost completely blocked due to the closure of access to the MXenes' working surface, despite the charge redistribution between the MXene film, water, and ethanol. The results of the calculation of the binding energy also indicated an unfavorable effect of high humidity, since water molecules are interconnected by hydrogen bonds, and prevent the resumption of chemoresistive properties of films.

**Author Contributions:** Conceptualization, O.E.G., D.A.K.; methodology, O.E.G.; funding acquisition, S.G.L.; investigation, O.E.G., D.A.K., S.G.L.; writing—original draft preparation, D.A.K., S.G.L.; writing—review and editing, O.E.G.; supervision, O.E.G. All authors have read and agreed to the published version of the manuscript.

**Funding:** The research was funded by the Russian Science Foundation, grant number 21-73-10251.

**Institutional Review Board Statement:** Not applicable.

**Informed Consent Statement:** Not applicable.

**Data Availability Statement:** Not applicable.

**Conflicts of Interest:** The authors declare no conflict of interest.

#### References

- Lu, J.; Persson, I.; Lind, H.; Palisaitis, J.; Li, M.; Li, Y.; Chen, K.; Zhou, J.; Du, S.; Chai, Z.; et al. Tin + 1Cn MXenes with fully saturated and thermally stable Cl terminations. *Nanoscale Adv.* **2019**, *1*, 3680–3685. [[CrossRef](#)]
- Kamysbayev, V.; Filatov, A.S.; Hu, H.; Rui, X.; Lagunas, F.; Wang, D.; Kile, R.F.; Talapin, D.V. Covalent surface modifications and superconductivity of two-dimensional metal carbide MXenes. *Science* **2020**, *369*, 979–983. [[CrossRef](#)] [[PubMed](#)]
- Mehdi Aghaei, S.; Aasi, A.; Panchapakesan, B. Experimental and Theoretical Advances in MXene-Based Gas Sensors. *ACS Omega* **2021**, *6*, 2450–2461. [[CrossRef](#)] [[PubMed](#)]
- Lee, E.; Kim, D.-J. Recent Exploration of Two-Dimensional MXenes for Gas Sensing: From a Theoretical to an Experimental View. *J. Electrochem. Soc.* **2020**, *167*, 037515. [[CrossRef](#)]
- Grützmacher, P.G.; Suarez, S.; Tolosa, A.; Gachot, C.; Song, G.; Wang, B.; Presser, V.; Mücklich, F.; Anasori, B.; Rosenkranz, A. Superior Wear-Resistance of Ti<sub>3</sub>C<sub>2</sub>T<sub>x</sub> Multilayer Coatings. *ACS Nano* **2021**, *15*, 8216–8224. [[CrossRef](#)]
- Marian, M.; Tremmel, S.; Wartzack, S.; Song, G.; Wang, B.; Yu, J.; Rosenkranz, A. MXene nanosheets as an emerging solid lubricant for machine elements—Towards increased energy efficiency and service life. *Appl. Surf. Sci.* **2020**, *523*, 146503. [[CrossRef](#)]
- Marian, M.; Song, G.C.; Wang, B.; Fuenzalida, V.M.; Krauß, S.; Merle, B.; Tremmel, S.; Wartzack, S.; Yu, J.; Rosenkranz, A. Effective usage of 2D MXene nanosheets as solid lubricant—Influence of contact pressure and relative humidity. *Appl. Surf. Sci.* **2020**, *531*, 147311. [[CrossRef](#)]
- Rosenkranz, A.; Grützmacher, P.; Espinoza-Gonzalez, R.; Fuenzalida, V.M.; Blanco, E.; Escalona, N.; Gracia, F.J.; Villarroel, R.; Guo, L.; Kang, R.; et al. Multi-layer Ti<sub>3</sub>C<sub>2</sub>T<sub>x</sub>-nanoparticles (MXenes) as solid lubricants—Role of surface terminations and intercalated water. *Appl. Surf. Sci.* **2019**, *494*, 13–21. [[CrossRef](#)]
- Huang, S.; Mochalin, V.N. Hydrolysis of 2D Transition-Metal Carbides (MXenes) in Colloidal Solutions. *Inorg. Chem.* **2019**, *58*, 1958–1966. [[CrossRef](#)]



10. Li, L.; Fu, X.; Chen, S.; Uzun, S.; Levitt, A.; Shuck, C.E.; Han, W.; Gogotsi, Y. Hydrophobic and Stable MXene-polymer Pressure Sensors for Wearable Electronics. *ACS Appl. Mater. Interfaces* **2020**, *12*, 15365–15369. [[CrossRef](#)]
11. Pei, Y.; Zhang, X.; Hui, Z.; Zhou, J.; Huang, X.; Sun, G.; Huang, W. Ti3C2TX MXene for Sensing Applications: Recent Progress, Design Principles, and Future Perspectives. *ACS Nano* **2021**, *15*, 3996–4017. [[CrossRef](#)] [[PubMed](#)]
12. Wu, M.; He, M.; Hu, Q.; Wu, Q.; Sun, G.; Xie, L.; Zhang, Z.; Zhu, Z.; Zhou, A. Ti3C2 MXene-Based Sensors with High Selectivity for NH3 Detection at Room Temperature. *ACS Sens.* **2019**, *4*, 2763. [[CrossRef](#)] [[PubMed](#)]
13. Koh, H.-J.; Kim, S.J.; Maleski, K.; Cho, S.-Y.; Kim, Y.-J.; Ahn, C.W.; Gogotsi, Y.; Jung, H.-T. Enhanced Selectivity of MXene Gas Sensors through Metal Ion Intercalation: In Situ X-ray Diffraction Study. *ACS Sens.* **2019**, *4*, 1365. [[CrossRef](#)]
14. Chae, Y.; Kim, S.J.; Cho, S.-Y.; Choi, J.; Maleski, K.; Lee, B.J.; Jung, H.-T.; Gogotsi, Y.; Lee, Y.; Ahn, C.W. An investigation into the factors governing the oxidation of two-dimensional Ti3C2 MXene. *Nanoscale* **2019**, *11*, 8387. [[CrossRef](#)]
15. Halim, J.; Kota, S.; Lukatskaya, M.R.; Naguib, M.; Zhao, M.-Q.; Moon, E.J.; Pitock, J.; Nanda, J.; May, S.J.; Gogotsi, Y.; et al. Synthesis and Characterization of 2D Molybdenum Carbide (MXene). *Adv. Funct. Mater.* **2016**, *26*, 3118. [[CrossRef](#)]
16. Guo, W.; Surya, S.G.; Babar, V.; Ming, F.; Sharma, S.; Alshareef, H.N.; Schwingenschlögl, U.; Salama, K.N. Selective Toluene Detection with Mo2CTx MXene at Room Temperature. *ACS Appl. Mater. Interfaces* **2020**, *12*, 57218. [[CrossRef](#)]
17. Wu, M.; Wang, B.; Hu, Q.; Wang, L.; Zhou, A. The Synthesis Process and Thermal Stability of V2C MXene. *Materials* **2018**, *11*, 2112. [[CrossRef](#)]
18. Zhang, Y.; Jiang, Y.; Duan, Z.; Huang, Q.; Wu, Y.; Liu, B.; Zhao, Q.; Wang, Q.; Yuan, Z.; Tai, H. Highly sensitive and selective NO2 sensor of alkaliized V2CT MXene driven by interlayer swelling. *Sens. Actuators B Chem.* **2021**, *344*, 130150. [[CrossRef](#)]
19. Wu, M.; An, Y.; Yang, R.; Tao, Z.; Xia, Q.; Hu, Q.; Li, M.; Chen, K.; Zhang, Z.; Huang, Q.; et al. V2CTx and Ti3C2Tx MXenes Nanosheets for Gas Sensing. *ACS Appl. Nano Mater.* **2021**, *4*, 6257–6268. [[CrossRef](#)]
20. Nahiriak, S.; Saruhan, B. MXene Heterostructures as Perspective Materials for Gas Sensing Applications. *Sensors* **2022**, *22*, 972. [[CrossRef](#)]
21. Lee, E.; Vahid-Mohammadi, A.; Yoon, Y.S.; Beidaghi, M.; Kim, D.J. Two-dimensional vanadium carbide MXene for gas sensors with ultrahigh sensitivity toward nonpolar gases. *ACS Sens.* **2019**, *4*, 1603–1611. [[CrossRef](#)] [[PubMed](#)]
22. Soler, J.M.; Artacho, E.; Gale, J.D.; García, A.; Junquera, J.; Ordejón, P.; Sánchez-Portal, D. The SIESTA method for ab-initio order-N materials simulation. *J. Phys. Condens. Matt.* **2002**, *14*, 2745–2779. [[CrossRef](#)]
23. Garcia, A.; Papior, N.; Akhtar, A.; Artacho, E.; Blum, V.; Bosoni, E.; Brandimarte, P.; Brandbyge, M.; Cerda, J.I.; Corsetti, F.; et al. SIESTA: Recent developments and applications. *J. Chem. Phys.* **2020**, *152*, 204108. [[CrossRef](#)] [[PubMed](#)]
24. Berland, K.; Hyldgaard, P. Exchange functional that tests the robustness of the plasmon description of the van der Waals density functional. *Phys. Rev. B* **2014**, *89*, 035412. [[CrossRef](#)]
25. Berland, K.; Arter, C.A.; Cooper, V.R.; Lee, K.; Lundqvist, B.I.; Schroder, E.; Thonhauser, T.; Hyldgaard, P. Van der Waals density functionals built upon the electron-gas tradition: Facing the challenge of competing interactions. *J. Chem. Phys.* **2014**, *140*, 18A539. [[CrossRef](#)] [[PubMed](#)]
26. Monkhorst, H.J.; Pack, J.D. Special points for Brillouin-zone integrations. *Phys. Rev. B* **1976**, *13*, 5188. [[CrossRef](#)]
27. Johnson, D.D. Modified Broyden's method for accelerating convergence in self-consistent calculations. *Phys. Rev. B* **1988**, *38*, 12807. [[CrossRef](#)]
28. Büttiker, M.; Imry, Y.; Landauer, R.; Pinhas, S. Generalized Many-Channel Conductance Formula with Application to Small Rings. *Phys. Rev. B* **1985**, *31*, 6207–6215. [[CrossRef](#)]
29. Rao, D.; Zhang, L.; Wang, Y.; Meng, Z.; Qian, X.; Liu, J.; Shen, X.; Qiao, G.; Lu, R.J. Mechanism on the Improved Performance of Lithium Sulfur Batteries with MXene-Based Additives. *Phys. Chem. C* **2017**, *121*, 11047–11054. [[CrossRef](#)]
30. Champagne, A.; Shi, L.; Ouisse, T.; Hackens, B.; Charlier, J.-C. Electronic and vibrational properties of V2C-based MXenes: From experiments to first-principles modeling. *Phys. Rev. B* **2018**, *97*, 115439. [[CrossRef](#)]
31. Lei, J.; Kutana, A.; Yakobson, B.I. Predicting stable phase monolayer Mo2C (MXene), a superconductor with chemically-tunable critical temperature. *J. Mater. Chem. C* **2017**, *5*, 3438–3444. [[CrossRef](#)]
32. Lu, H.; Dai, D.; Yanga, P.; Lic, L. Atomic orbitals in molecules: General electronegativity and improvement of Mulliken population analysis. *Phys. Chem. Chem. Phys.* **2006**, *8*, 340–346. [[CrossRef](#)] [[PubMed](#)]
33. Pazniak, H.; Varezchnikov, A.S.; Kolosov, D.A.; Plugin, I.A.; Di Vito, A.; Glukhova, O.E.; Sheverdyayeva, P.M.; Spasova, M.; Kaikov, I.; Kolesnikov, E.A.; et al. 2D Molybdenum Carbide MXenes for Enhanced Selective Detection of Humidity in Air. *Adv. Mater.* **2021**, *33*, 2104878. [[CrossRef](#)] [[PubMed](#)]